SEEJ: SmallSat Exosphere Explorer of Hot Jupiters

Scott J. Wolk, JaeSub Hong, Suzanne Romaine, Katja Poppenhaeger, Almus Kenter, et al.

Scott J. Wolk, JaeSub Hong, Suzanne Romaine, Katja Poppenhaeger, Almus Kenter, Althea V. Moorhead, Dennis L. Gallagher, Christopher S. Moore, Martin Elvis, Ralph Kraft, Jeremy Drake, Vinay Kashyap, Elaine Winston, Bradford Wargelin, Ignazio Pillitteri, Diab Jerius, Mark Stahl, Bruce Wiegmann, Christopher Loghry, "SEEJ: SmallSat Exosphere Explorer of Hot Jupiters," Proc. SPIE 11118, UV, X-Ray, and Gamma-Ray Space Instrumentation for Astronomy XXI, 111180E (9 September 2019); doi: 10.1117/12.2529380

SPIE.

Event: SPIE Optical Engineering + Applications, 2019, San Diego, California, United States

SEEJ: *SmallSat Exosphere Explorer of Hot Jupiters*

Scott J. Wolk*[a], JaeSub Hong[a], Suzanne Romaine[a], Katja Poppenhaeger[b], Almus Kenter[a], Althea V. Moorhead[c], Dennis Gallagher[c], Christopher S. Moore[a], Martin Elvis[a], Ralph Kraft[a], Jeremy Drake[a], Vinay Kashyap[a], Elaine Winston[a], Bradford Wargelin[a], Ignazio Pillitteri[d], Diab Jerius[a], Mark Stahl[c], Bruce Wiegmann[c], Christopher Loghry[e]

[a]Harvard-Smithsonian Center for Astrophysics, 60 Garden St., Cambridge, MA, 02138, USA;
[b]Leibniz Institute for Astrophysics Potsdam, An der Sternwarte 16,14482 Potsdam, Germany;
[c]NASA Marshall Space Flight Center, Huntsville, AL, 35808, USA;
[d]INAF-Osservatorio Astronomico di Palermo, Piazza del Parlamento 1, 90134 Palermo, Italy;
[e]Moog Inc, Space and Defense Group, Chatsworth, CA, 91311, USA

ABSTRACT

The first detected exoplanets found were "hot Jupiters"; these are large Jupiter-like planets in close orbits with their host star. The stars in these so-called "hot Jupiter systems" can have significant X-ray emission and the X-ray flux likely changes the evolution of the overall star-planetary system in at least two ways: (1) the intense high energy flux alters the structure of the upper atmosphere of the planet - in some cases leading to significant mass loss; (2) the angular momentum and magnetic field of the planet induces even more activity on the star, enhancing its X-rays, which are then subsequently absorbed by the planet. If the alignment of the systems is appropriate, the planet will transit the host star. The resulting drop in flux from the star allows us to measure the distribution of the low-density planetary atmosphere. We describe a science mission concept for a SmallSat Exosphere Explorer of hot Jupiters (SEEJ; pronounced "siege"). SEEJ will monitor the X-ray emission of nearby X-ray bright stars with transiting hot Jupiters in order to measure the lowest density portion of exoplanet atmospheres and the coronae of the exoplanet hosts. SEEJ will use revolutionary Miniature X-ray Optics (MiXO) and CMOS X-ray detectors to obtain sufficient collecting area and high sensitivity in a low mass, small volume and low-cost package. SEEJ will observe scores of transits occurring on select systems to make detailed measurements of the transit depth and shape which can be compared to out-of-transit behavior of the target system. The depth and duration of the flux change will allow us to characterize the exospheres of multiple hot Jupiters in a single year. In addition, the long baselines (covering multiple stellar rotation periods) from the transit data will allow us to characterize the temperature, flux and flare rates of the exoplanet hosts at an unprecedented level. This, in turn, will provide valuable constraints for models of atmospheric loss. In this contribution we outline the science of SEEJ and focus on the enabling technologies Miniature X-ray Optics and CMOS X-ray detectors.

Keywords: exoplanets, Flares, Stars, X-rays, Space Missions, SmallSat, X-ray optics, X-ray detectors: CMOS

1. INTRODUCTION

The SmallSat Exosphere Explorer of hot Jupiters (SEEJ; pronounced “siege”) will measure the maximum extent of the atmospheres of Hot Jupiters. SEEJ will advance our understanding of the physical processes and consequences of the strong interactions taking place between the outer atmospheres of exoplanets and the coronae of their stellar hosts. Specifically, the SEEJ investigation will determine how much stellar high-energy photon flux inflates nearby exoplanet atmospheres. The investigation will determine the bulk composition of the inflated atmosphere and will assess the presence of dense evaporation tails resulting from this interaction. These science objectives will be accomplished using new, revolutionary Miniature X-ray Optics that provide near-Chandra collecting area in a low-mass, small-volume, and low-cost package. The operational objective is for SEEJ to observe roughly 50 transits of up to 7 X-ray bright exoplanet hosts in a single year.

The discovery of exoplanets has fundamentally changed our perception of the universe and humanity’s place within it. The first and most easily detected exoplanets were “hot Jupiters” which are large Jupiter-like planets in close orbits around their host star. In the cases of stars with significant X-ray emission, the X-ray flux can alter the structure of the upper

*swolk@cfa.harvard.edu;

UV, X-Ray, and Gamma-Ray Space Instrumentation for Astronomy XXI, edited by Oswald H. Siegmund, Proc. of SPIE
Vol. 11118, 111180E · © 2019 SPIE · CCC code: 0277-786X/19/$21 · doi: 10.1117/12.2529380

atmosphere of the planet, potentially blowing it away. Meanwhile, the angular momentum and magnetic field of the planet induces even more activity on the star, further enhancing its X-ray emission.

X-ray absorption during a transit acts as a unique and valuable probe of the planetary exosphere. Using Chandra, Poppenhaeger, Schmitt & Wolk [Fig:1] monitored multiple transits of the hot Jupiter HD189733b in X-rays and measured a transit depth of 7%, three times deeper than the ~2% optical eclipse depth, implying that the atmosphere is opaque to soft X-rays (< 1keV) out to twice the optical radius of the planet. This discovery shows that, with existing technology, the extended atmospheres of hot Jupiters can be characterized, and asymmetries measured. This improved understanding can, in turn, constrain the loss of atmospheres in exo-Earths around M-stars, an important issue for exobiology.

(1) The Primary Objective of SEEJ is to measure the extent of exoplanets' atmospheres via measurement of the depth, width and shape of the exoplanet transit x-ray light curve.

The star itself is of course critical to the atmosphere of the planet. Specifically, X-rays can induce both life-enabling and life-threatening photochemistry in planetary atmospheres. Similarly, observed X-ray flares may be harbingers of coronal mass ejections which can aid life by removing primary, hydrogen-dominated, atmospheres or threaten its existence by depleting secondary atmospheres. It is therefore vital to understand the general behavior of stellar coronae at all phases of stellar/planetary evolution to gauge to the cumulative impact of stellar X-rays on planetary atmospheres.

(2) The Secondary Objective of SEEJ is to quantify the activity of the stellar hosts through sustained monitoring.

SEEJ will repeatedly monitor exoplanet transits in X-rays to build up adequate signal to provide detailed transit light curve profiles of suitable targets discovered by TESS. Carrying a quartet of specialized telescopes using Miniature X-ray Optics (MiXO) and CMOS sensors developed at the Smithsonian Astrophysical Observatory (SAO) and NASA Marshall Space Flight Center (MSFC), together providing a net collecting area comparable to that of Chandra. ***SEEJ will monitor roughly 50 transits of about 7 X-ray bright exoplanet hosts in a single year.***

NASA Marshall Space Flight Center (MSFC)'s Advanced Concepts Office (ACO) developed the SEEJ spacecraft concept, which will be implemented by MOOG industries. MSFC/ACO performed a comprehensive analysis of all aspects of the SEEJ mission. Costs were estimated using parametric analysis and found to be consistent with the 35-million-dollar cost cap.

2. THE SCIENCE OF SEEJ

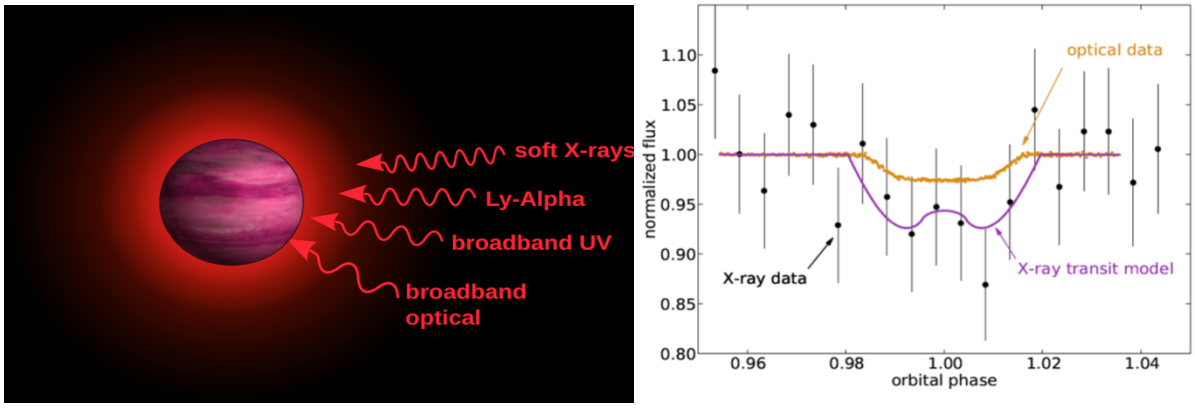

Figure 1: (**Left**) Schematic of the absorption altitudes in the atmosphere of a Hot Jupiter (HD 189733b). (**Right**) X-ray transit light curve composed of 5 summed Chandra observations in comparison with optical transit data; vertical bars denote 1σ error bars of the X-ray data. The purple curve shows the best fit to a limb-brightened transit. The X-ray data are rebinned to phase bins of 0.005 [1]. SEEJ will obtain more than 10 times this number of transits, and so will yield 3 times smaller error bars for about a dozen hot Jupiter systems.

2.1 Primary Science Objective

The Primary Science Objective of SEEJ is to measure the extent of exoplanets' atmospheres via measurement of the depth, width and shape of the exoplanet transit x-ray light curve from 0.3-2.0 keV. Using high cadence monitoring SEEJ will observe scores of transits of each X-ray bright system achieving signal to noise similar to, or better than, published results from Chandra. Many identified exoplanets are so-called Hot Jupiters because they have gas giant masses (~10^{27}kg;), yet are closer to their host stars than Mercury is to the Sun, with orbital periods of < 10 days, and so have surface temperatures >1000 K. This is a hostile environment for a gas dominated planet. The inclusion of stellar X-ray and UV flux in irradiance calculations leads to energy-limited escape and atmospheric expansion not found in models incorporating Jeans escape or stellar UV/optical/IR insolation alone. The increased mass loss rates are of order 10^{12} g s^{-1}, implying hydrogen-rich giant exoplanets may lose 10% of their mass on a timescale of ~1 Gyr, just ~1/5 the age of the Solar System. In this model, the high-energy radiation is absorbed in the upper layers of the planetary atmosphere, which consequently heat to temperatures in excess of 10 000 K, too hot to remain bound to the planet. A hydrodynamic outflow forms guided by the large scale stellar inter-planetary magnetic field, similar to the classic Parker model of the solar wind. This mechanism can produce mass-loss rates which are qualitatively corroborated by UV observations of actual exoplanetary mass-loss in hot Jupiters with large amounts of hydrogen and helium in their atmospheres [2]. Knowing the atmospheric mass-loss requires measuring the exoplanetary high-energy environment in more detail than UV observations alone can ever supply.

The generation of an exosphere due to local X-ray irradiation has been directly detected in two cases, the planets HD 209458b (in UV) and HD 189733b (in UV and X-ray). Absorption of high energy photons by atmospheric gas has been used to probe the layer where the gas escapes in the upper atmosphere [1, 3, 4]. Modeling shows evolution of close-in exoplanets strongly depends on the detailed X-ray luminosity history of their host stars [5]. Stars with an X-ray luminosity > 10^{30} erg cm^{-2} s^{-1} (~1000x that of the Sun) evaporate most of their planets' atmospheres within 0.05 AU. Conversely, a significant fraction of atmospheres can survive more moderate X-ray luminosities. At X-ray luminosities lower than that of the Sun (<10^{27} erg cm^{-2} s^{-1}), the mass loss is negligible for hydrogen-rich Jupiter-mass planets at >0.02 AU, while Neptune-mass planets are influenced out to 0.05 AU [6].

A major unknown is the density of the extended planetary atmosphere. UV techniques reveal relatively dense atmospheric layers extending perhaps $0.1R_{jup}$ above the optical cloud tops [3]. The X-ray observations detect material at densities as low as 10^{9} cm^{-3}, corresponding to atmospheric layers extending further than $0.75R_{jup}$ above the cloud tops. The density of this material is too low to be measured by UV techniques. While HST observations have shown a slightly enhanced transit depth in hydrogen Ly-α [3, 7], the high temperatures in the exoplanet exospheres typically cause a large fraction of the hydrogen to be ionized, so Ly-α based exosphere density estimates range over eight orders of magnitude (column densities of 10^{13} - 10^{21} cm^{-2} [8]). Only with spectrally resolved X-ray transit measurements, such as those envisioned by SEEJ, will the density be unambiguously determined.

Most of the X-ray absorption in an atmosphere of solar chemical composition is due to Nitrogen and Oxygen, which have large cross-sections only below 1 keV (N K-edge 0.40 keV; O K-edge 0.53 keV). These edges can be detected with the intrinsic energy resolution of CMOS X-ray detectors. The collecting area of Chandra ACIS-S at the Oxygen edge was about 110 cm^2 at the time of the HD 189733 observations. Just 5 "clean" transit observations were needed to obtain the signal to noise shown in figure 1. Each MiXO is optimized to provide about 40 cm^2 at 1 keV. SEEJ will use a quartet of such telescopes Thus, a dedicated mission can duplicate a Chandra observation, by using ~8 times more transits.

2.2 Secondary Science Objective:

The secondary objective of SEEJ is to measure flare activity of the host star through long term high cadence monitoring. Existing data indicate that most host Jupiters are inflated beyond the value expected due to photospheric blackbody luminosity alone. Analysis has demonstrated that this is due to X-ray and extreme UV flux (XUV) [6]. This XUV flux also leads to critical photochemistry in planetary upper atmosphere and changes the overall thermal budget [9,10]. Coronal mass ejections (CMEs), which are currently best noted through their X-ray emission, could have even more significant effects on the planetary atmosphere [2, 11]. A single flare was observed emanating from HD 189733A which the data indicted spaned a significant fraction of the star-planet distance; It appeared that the planet may have been acting as a footpoint of the flare [12]. Fulton et al. investigated the process of heating and inflation in relation to the observed gaps in the distribution of known exoplanets in the Radius vs. Orbital Period diagram. They identify two features referred to as the 'Evaporation Gap' and the 'Evaporation Valley' where there is a scarcity of lower-mass gas giant planets in orbits with smaller stellar radii [13, 14]. They determined that the scarcity of sub-Neptunes is due to exposure to the

high energy fluxes from their host stars. UV and X-ray fluxes scale with stellar masses, as do planetary masses, in such a way that lower -mass gas giants cannot retain their atmospheres close to brighter stars and so they photo-evaporate due to XUV flux. In short, knowing the XUV emission from the host star is critical to our ability to understand exoplanet atmospheres.

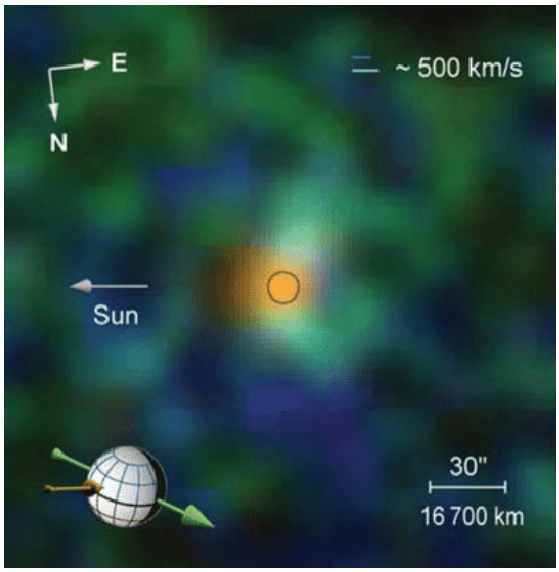

Figure 2: XMM-Newton image of Mars showing exospheric material being evaporated by the solar wind. Ionized oxygen is coded in blue, ionized carbon is coded in green. Both of these features are extended leeward with respect to the solar wind. Fluorescence oxygen is coded in yellow and red shows no motion. The circle indicates the position and size of Mars; the projected direction of the Sun is towards the left [17].

When not observing transits, *SEEJ* will monitor the transit hosts through the full range of orbital and synodic phases and use the comprehensive knowledge of the energetic photon environment to understand the energy balance of the planetary exosphere. In a single year we expect over a million seconds of monitoring time of each star. The data will allow a very precise measurement of the average flux from the host star as well as an evaluation of the range of X-ray fluxes incident on the exoplanet. Just as importantly, SEEJ will be able to establish an unbiased flare rate and a detailed flare spectrum. That is, the distribution of intensities, durations and temperatures of the flares from each star.

2.3 Synergy Between the Science Objectives

A particular strength of observing exoplanets in the X-ray regime is that the same measurement, i.e. the star-planet system's X-ray flux over time, contains information about both the exoplanet's atmosphere and the driver of atmospheric evaporation, namely the stellar magnetic activity. Magnetic activity and the stellar X-ray and UV flux it causes have long been suspected to be the driving force behind exoplanetary mass loss based on theoretical considerations [15]. There is also accumulating observational evidence for this. Evaporation of exoplanetary helium has been observed for planets with high-activity host stars (for example [11, 16]), while restrictive upper limits on helium evaporation have been placed on exoplanets around lower-activity host stars [16].

Measuring the inflation and evaporation of exoplanetary atmospheres and the intensity of the planetary X-ray irradiation simultaneously by design, SEEJ will allow us to study how exoplanetary high-altitude atmospheres behave as a function of the host stars' activity. Additional stellar activity markers like flaring behavior and coronal temperatures will provide additional parameters to characterize the stellar activity and how it related in more detail to evaporation.

2.4 Target Selection

The targets of SEEJ will be X-ray bright solar type stars with a transiting hot Jupiter as well as lower mass, more nearby stars with transiting "hot Neptunes". Overall, there are about 14,000 RASS sources with V < 11.5 [18]; TESS is currently in the process of a fully survey for such sources. Statistically, it is estimated that about 1% of stars host a hot Jupiter [19]. Thus, about 140 RASS/TESS sources will host hot Jupiters. Geometric arguments indicate the probability of a transit in such systems is about 15%. While there is some uncertainty in the exact number of hot Jupiters which will be found around X-ray bright sources, the bias appears in favor of an increased likelihood of the host being X-ray bright due to star-planet interactions. Overall, we expect about 20 X-ray bright transiting hot Jupiter hosts with $F_x > 2.5 \times 10^{-12}$ erg cm^2 s^{-1} (0.5-2.0 keV) to be identified by TESS. This number will be solidified by the end of the primary TESS mission in 2020. With the advent of eROSITA we expect to lower the X-ray flux limit by an order of magnitude, thus significantly increasing the number of possible SEEJ targets.

Typically, a hot Jupiter has an orbital period of about 4 days, so each will transit ~90 times per year. Each transit lasts only 2-3 hours. With 7 targets there will be about 1500 hours of transit time over the course of a year. In the best case, if a planet has a 4-day period and is continuously visible, we could observe 75 transits.

2.5 Mission Requirements

A combination of analytic and simulation analyses demonstrate that the above described science can be accomplished with a relatively modest satellite. The primary requirement is at least 50 cm^2 of collecting area in the soft X-ray band (0.3-2.0 keV). Modest energy resolution (150 eV) will be used to measure the energy dependence of planetary atmospheric absorption, providing constraints on chemical composition, plasma temperatures and help distinguish flares from random fluctuations. Moderately good (30" half-power diameter) spatial resolution will allow SEEJ to isolate individual stars and maintain a manageable background flux rate. While a field of view of at least 5 arc minutes on a side will allow the capture of all the X-ray energy and still have a significant fraction of the field available for background evaluation. In the next section we describe the instrumentation which will enable SEEJ.

2.6 The Need for SEEJ

The time is right for a mission like *SEEJ*. While results from the WASP survey indicate most hot Jupiters around nearby F and early G stars may have been found, NASA's TESS Spacecraft was launched with the specific goal of finding close in planets around nearby later type G-, K-, and M stars that are brighter than 12^{th} magnitude. By summer 2020 *TESS* will have completed its primary mission and will have discovered more than 20,000 transiting exoplanets, most of which will be Jupiter, Saturn, and Neptune sized planets in the so-called "hot" zone with periods less than 10 days. We will be able to pick out X-ray bright (>2.5 $x10^{-12}$ ergs cm^{-2} sec^{-1}) sources from these by comparing with the ROSAT All Sky Survey. The recently launched eROSITA experiment promises access to a half-sky survey to ten times this depth. In the meantime, *Chandra* and *XMM-Newton* can be used to evaluate promising targets. By cross-matching with Gaia, we can determine their true distances.

While *Chandra*, *Swift*, *XMM-Newton* and (eventually) *XRISM* can evaluate targets for *SEEJ*, they cannot replace the mission. The critical features that drive SEEJ are low-energy collecting area, which can characterize exospheric absorption, and multiple repeated observations, which are necessary to account for variable stellar activity. Hard X-rays (>2 keV) are highly penetrating and absorbed deep in the atmosphere, similar to optical photons and so are of limited scientific interest regarding the atmospheres of exoplanets. Conversely, in the soft X-ray regime, absorption is a strong function of energy. The same transit can appear twice as deep at 300 eV than at 800 eV. Furthermore, most stellar coronae are relatively cool with little emission at higher energies except during extreme flares. As discussed below, *SEEJ* is designed to have about 100 cm^2 effective area at the oxygen feature near 600 eV (**Fig. 4**). The other missions mentioned are designed to look at relativistic phenomena and have effective areas optimized for hard X-ray bands. For example, the Swift/XRT has an effective area of 30 cm^2 at 600 eV, Chandra/ACIS < 10 cm^2 at 600 eV, XRISM/Resolve ~50 cm^2 at 600 eV. Among existing pointing missions, and those planned through the middle of the next decade, only the combined EPIC/MOS+PN of *XMM-Newton* has adequate energy discrimination and exceeds SEEJ in effective area in this wavelength regime. Even *XMM-Newton*, however, is severely constrained in its mission scheduling parameters such that long-term monitoring of both the transit epochs as well as that of pre- and post-transit observations to determine baseline stellar emission levels is prohibitively expensive. With SEEJ, we will also obtain observations covering complete planetary orbits which can address issues like the existence and magnitude of the Star-Planet Interaction (SPI) effect.

3. INSTRUMENTATION

Packaged to fit within the ESPA bus and taking advantage of two new enabling technologies, *SEEJ* carries four identical Compact X-ray Imaging Spectrometers (CXIS) as shown in **Fig. 3** to meet the science requirements and to achieve the desired performance. The CXIS is a lightweight Wolter-I X-ray telescope in a small form factor, with a Miniature X-ray Optics (MiXO) module and a monolithic CMOS X-ray sensor. A common backend electronics module with a Controller Board (CTB) powers and controls the four focal plane CMOS detectors, and processes their data.

Table 1 summarizes the key instrument parameters of one CXIS module. The CXIS is optimized for capturing 0.5–1.5 keV soft X-rays with full response covering 0.3–2 keV and <120 eV FWHM spectral resolution. The combined effective area of the four CXIS modules is ~140 cm^2 at 1 keV (optics collecting area ~ 170 cm^2). The CXIS modules are co-aligned to cover the same 10 arcmin diameter field of view (FOV) with 25 arcsec Half-Power Diameter (HPD).

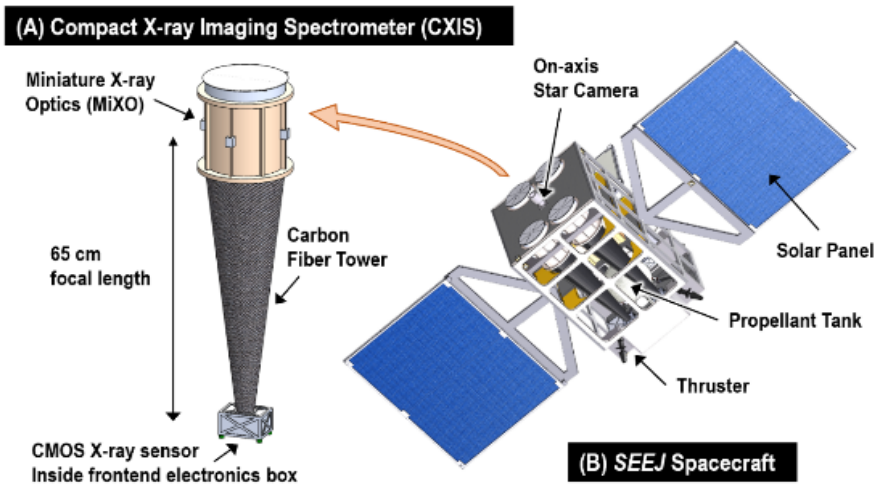

Figure 3: ***(A)*** Compact X-ray Imaging Spectrometer (CXIS) onboard ***(B)*** the SEEJ Spacecraft. SEEJ carries four identical CXIS to meet the science requirements. Each CXIS consists of a Miniature X-ray Optics (MiXO) module and a CMOS X-ray sensor at the focal plane.

3.1 Miniature X-ray Optics (MiXO)

Nearly all modern X-ray astronomy missions have been designed around grazing-incidence optics with Wolter-I geometries [20]. The Wolter-1 configuration combines reflections, first from a parabolic, then from a hyperbolic surface to reduce off-axis aberrations (over a single bounce system) for imaging. To increase the collecting area of these telescopes, several barrel shaped mirrors of varying diameter can be nested one inside the other along the same optical axis.

The *SEEJ* X-ray optic module, shown in **Fig. 4**, consists of Wolter-I X-ray mirrors, a spider alignment fixture, an outer housing, a thermal shield (TS), an extendable baffle, and a protective cover. The TS, placed in front of the telescope and working in conjunction with an electric heater attached to the optics housing, provides thermal control of the optics (+20 ± 1 °C). Its design is similar to those used on previous X-ray missions such as *Suzaku*, *Hitomi*, and *XMM-Newton* [21, 22, 23]. A stray light baffle is used to reduce the background due to light coming directly through between the individual shells. The optics cover, common to all four modules, protects the TS during launch.

Each aluminum mirror module housing contains 15-20 nested shells, attached at their front ends to an 8-spoke spider assembly. The spider arms have machined grooves into which the shells are epoxied during the alignment process. The spider is made of a nickel alloy which closely matches the coefficient of thermal expansion (CTE) of the mirror shells. A 3-spoke spider at the back end of the shells secures the structure. It is not epoxied to the shells (and thus does not support them), as the additional constraint would induce optical distortions.

Replication of X-ray Optics and Heritage: The X-ray mirrors are fabricated using an electroformed nickel replication (ENR) technique which has been successfully used to fabricate optics for several X-ray astronomy missions such as Swift/XRT, XMM-Newton, Spectrum-RG, and FOXSI [24, 25]. The surface and figure of the mandrel are replicated by the optic; good quality X-ray optics require both low (<5Å) surface microroughness and good (< 15 arcsec HPD) mandrel figure. To date, nickel electroforming is the method that has produced the best replicated mirrors. The sequence of process steps for mandrel preparation and mirror shell fabrication of ENR optics is shown in Figure 4-5. In this process, thin nickel or nickel-alloy shells are electroformed onto figured and polished electroless-nickel-plated aluminum mandrels from which they are later separated by differential thermal contraction. The resulting optics are full shells of revolution which makes them inherently stable with good figure control and good angular resolution, and their alignment is also relatively straightforward. The mandrels are fabricated by Marshall Space Flight Center (MSFC) and delivered to SAO where the individual nickel shells are fabricated and coated. The finished shells are then delivered from SAO to MSFC where they are aligned into the mirror fixture. The completed module is tested in X-rays at MSFC in the 100-m-long Stray-Light facility (SLF). SAO has collaborated with MSFC over the past 20 years to develop multilayer coated X-ray optics for astrophysics and ground-based programs; SEEJ leverages this long-standing collaboration to develop small form X-ray optics for other applications [26, 27].

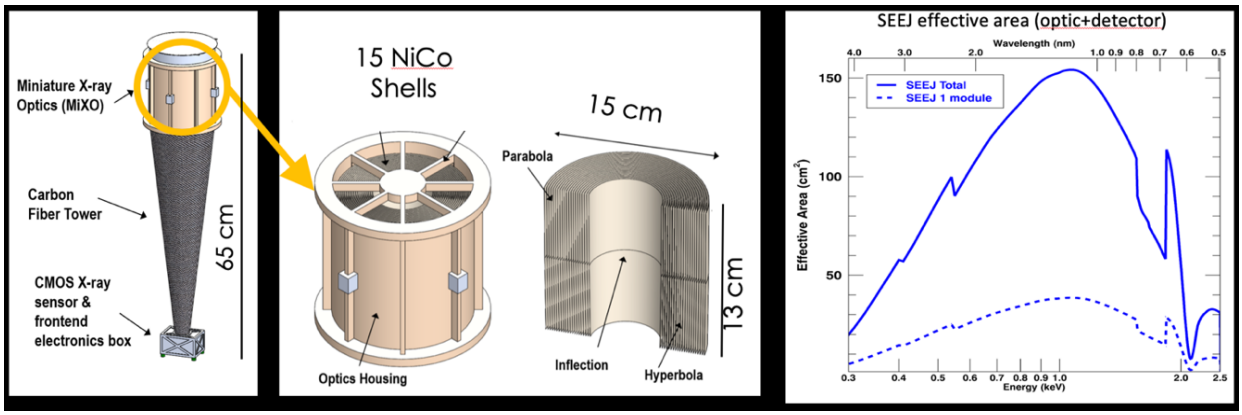

Figure 4: Design concept for SEEJ focal modules (FM). Left: optics shown in housing with alignment spider. Middle: 15 nested shells. Right: Effective area optic+detector (no OBF or thermal Shield) for 1 and 4 CXIS. Not shown in this drawing are the thermal shield. There will also be a protective launch cover shared by the four telescopes.

The SEEJ team has fabricated many single-shell optics for other applications which have smaller diameter and smaller length than the SEEJ design; however, these were not assembled for flight or tested in a relevant environment. ENR X-ray optics modules with 25 and 20 arcsec angular resolution (HPD) have been fabricated for missions such as ART-XC [28] and FOXSI [29] respectively, using shell thicknesses of 240 µm. Similar thickness and shell spacing is designed for SEEJ as shown in Table 1.

SAO in collaboration with MSFC and a few industry partners has multiple programs to develop replicated optics for a number of applications [30, 31]. Among these, Miniature X-ray Optics (MiXO) for planetary application is funded for development under a NASA PICASSO program (grant NNX16AL75G) [e.g., 30, 31] The primary objective of the PICASSO effort is to develop small and lightweight ENR mirror shells suitable for planetary applications. The SEEJ optics will leverage heavily on work being carried out under the PICASSO program. Mandrels for the PICASSO program are shown in Figure 5 along with a nested pair of shells replicated from these mandrels. Metrology of the mandrels indicates a figure of 15 arcsec.

Table 1 Key Instrument parameters

Parameters	One CXIS Module
Main Subsystems	MiXO + CMOS + backend electronics
Volume & Mass	~20×20×80 cm, 6.8 kg (26 kg*)
Power	7.4W normal/10.4W peak (21W normal/30W peak*)
Data Rate	0.8 GB/wk (3.2 GB/wk*)
Focal Length	65 cm
Ang. Res. & FOV	25 arcsec HPD, 10 arcmin dia.
MiXO+CMOS Combined Eff. Area	≥35 cm^2 @ 1 keV (≥140 cm^2 @ 1 keV*)
Energy Res. & Range	<120 eV @ 1 keV, 0.3 – 2 keV
Timing Resolution	≲ 50 ms
Instrument Thermal Control	Passively with radiators & heaters: +20 ± 1°C for MiXO; T_o ± 2°C for CMOS**

* *SEEJ* total: 4 CXIS + backend electronics

** T_o: ~–20°C to 0°C

The effective area of grazing incidence optics is dictated both by the size of the optics and the number of nested shells. The geometric area of optics allocated for CubeSats/SmallSats and planetary missions is necessarily limited, therefore one would like to nest the maximum number of shells into the optics module to maximize the effective area and minimize the observing time. However, there is a limit to the minimum shell thickness and minimum packing distance between shells. The minimum shell thickness is limited by the stress induced during the separation process and the deformation that can be induced during the mounting process. The minimum packing distance is due to the space needed for aligning and fixturing the nested shells into the module.

Figure 5: Left: Existing MiXO mandrels. Mandrel diameters 9 cm, 10 cm; length = 9 cm. Mandrel figure 15 arcsec. (Red gaskets are used between optic and end-rings during plating. See text for more detail.) Center: Nested shells replicated from the two mandrels. FWHM of individual optics measured < 20 arcsec at MSFC SLF. Right: CCD image from optic tested at MSFC SLF. FWHM is < 20 arcsec.

3.1.1 Performance estimation of the SEEJ MiXO module

Preliminary modelling shows that 15 shells will meet the effective area goal of 140 cm^2; the final number of shells (between 15 and 20) will be set during Phase A after more detailed modelling. To meet the effective area required by L1 science, the X-ray optics outer diameter is set to 15 cm diameter with 13 cm length. A model was constructed to determine the optimal shell length that minimizes the number of shells while keeping the angular resolution <~ 30 arcsec in HPD, as required by L1 science. Figure 4 shows the effective area vs. energy for the SEEJ optics with 15 NiCo shells. The effective area is calculated for X-rays only within a 1 arcmin enclosure radius around each off-axis point in the detector.

SEEJ shells have a focal length four times smaller and are five times shorter than for other missions. While the shorter length shells pose tighter constraints in the alignment and fixturing (e.g., tilt errors are less forgiving in shorter shells with shorter focal length), the proposed SEEJ mission has more forgiving requirements (e.g., HPD requirements of 30 – 50 arcsec for SEEJ vs. currently achievable 15 arcsec for longer optics). Alignment of the shells introduces additional error terms in angular resolution due to deformation during the mounting of the shell in the spider. Based on the fabrication history of similar optics modules, Table 2 shows the expected angular resolution after taking into account the expected error at each stage of the fabrication. MSFC has recently developed a new mounting and alignment system which has improved the process considerably for larger X-ray optics [28]. We expect this improvement to carry over to the alignment of the small optics; if this is the case, the numbers quoted above will improve further.

Table 2 Key parameters of optics modules for X-ray missions

Mission	Focal length (cm)	Shell length (cm)	Shell spacing (mm)	Inner diameter (mm)	Outer diameter (mm)	Shell thickness (μm)	No. of shells	Coating thickness
SEEJ	**65**	**13**	**1.8**	**88**	**150**	**250**	**20**	**Ir, 300Å**
FOXSI	200	60	1.8	63	103	240	10+	Ir, 300Å
ART-XC	270	60	1.8	50	150	240	28	Ir, 300Å
IXPE	400	60	1.8	162	272	180-260	24	Bare Ni

3.2 Focal Plane CMOS X-ray sensors and backend electronics

The SEEJ focal plane will employ four CMOS imagers each matched to a separate MiXO optic. Each CMOS sensor will have its own headboard and will be driven by a single common Controller Board (CTB, aka the "Motherboard"). The CMOS sensors will be in flight molybdenum packages provided to the SEEJ program by SRI. The cover of the package will incorporate a 10-arcminute wide circular aperture to define the science FOV. That cover will also house an on-orbit ^{55}Fe calibration (Fig. 6) source, which will be sufficiently removed from, and collimated so as not to interfere with the science ROI. The optical blocking filter (OBF) will cover the circular aperture and it will limit the out-of-band optical and UV photon flux. SEEJ will employ four CXIS modules, each with MiXO + OBF + CMOS, achieving >100 cm^2 effective

area between 0.5–1.5 keV, which is required to meet the scientific objectives. Each of the four CMOS instruments will be extensively calibrated at the SAO X-ray facility (SAO-XRF).

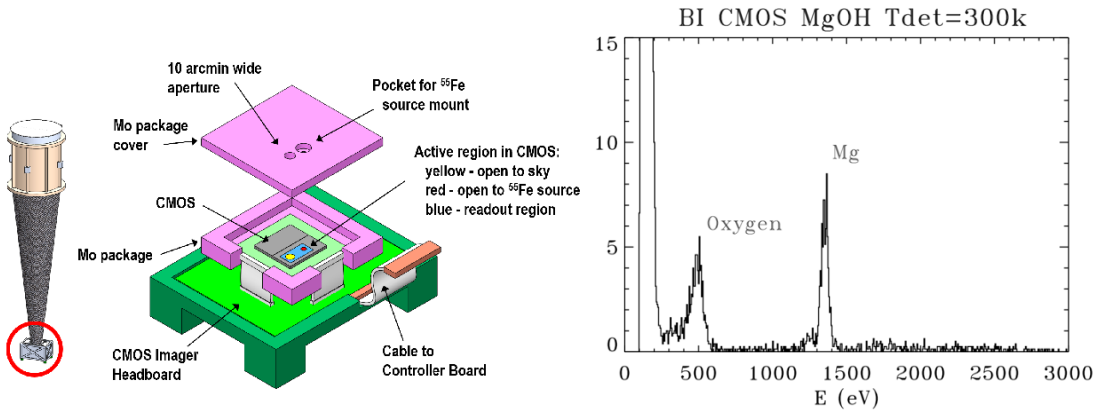

Figure 6: **Left**: Focal plane CMOS X-ray sensor arrangement of a SEEJ CXIS module. **Right**: MgO measurements made at the SAO test facility. CMOS can easily resolve the emission from Mg (near 1.24 keV) and O (near 0.525 keV) which are in the primary SEEJ science bandpass 0.3 - 2 keV.

CMOS imaging sensors, once relegated for use in consumer items such as "web-cams" and cell phones, have been greatly improved and are now replacing CCDs in many scientific and astronomical applications. New scientific grade CMOS devices have demonstrated read-noise levels comparable to the best CCDs, and like CCDs, CMOS imagers are now regularly available back-thinned for Back Illumination (BI). Back thinning greatly increases QE while eliminating the Fixed Pattern Noise (FPN) caused by the partially opaque and extensive front-side CMOS circuitry. Back thinning and processing of either CMOS or CCDs is a virtually identical and well-established process. For a soft X-ray CMOS application such as SEEJ, BI is particular important as front side versions of BMIII CMOS imagers show an effective dead layer equivalent to ~7um of SiO_2 which would significantly reduce X-ray QE below 1keV.

Scientific CMOS imagers are well-suited to be the next generation of pixelated Si detectors for space-based optical, IR and X-ray telescopes due to their performance, operational simplicity, inherent tolerance to radiation and high levels of integration. The candidate CMOS X-ray Active Pixel Sensor (APS) for the SEEJ mission focal plane is known as the "Big Minimal III" (BM-III). These BM-III CMOS devices were designed by SRI International ("Sarnoff"), fabricated and tested with funding provided by a NASA/APRA program (NNX09AE86G), a grant from the Betty and Gordon Moore foundation, and internal Smithsonian Institute (SI) resources [32]. The BM-III share a common heritage with the flight CMOS imagers provided by SRI for other programs [33,34] such as SoloHi, WISPR [35], and the Europa Imaging System (EIS) [36].

Here we summarize the main characteristics expected from previous testing. The low power consumption (typically ~10 mW per device) and very fast full frame (> 40 Hz) and proportionally much faster subframe read-out of these CMOS devices mitigate the contribution of dark current (< 1e^-pix at read rate); the thermal control and cooling requirements (-20–20 C operational temperatures) are therefore modest compared to CCDs—a feature very suitable for any resource-limited mission like SEEJ. Similarly, the fast readout makes it possible to have a thinner OBF which increases overall X-ray detector QE particularly below 1 keV. The fast readout also provides the temporal dynamic range required for observing bright, highly variable X-ray emission, mitigating any photon pile-up. The small pixel size16 µm (corresponding to ~4 arcsec per pixel for a focal length of 70 cm) is sufficient to over-sample the SEEJ MiXO point spread function (PSF ~30 arcsec HPD on-axis). Each "Transfer Gate" pixel has its own collection node, sense node, and source follower amplifier (Fig. 7); hence charge to voltage conversion occurs at the pixel. The CMOS process is inherently radiation tolerant (>100 krads) as the thin CMOS insulator layers are not susceptible to cause flat-band shifting and, unlike CCDs, there is no need for long charge transfers. CMOS devices are therefore well-suited to space applications.

The BM-III device is comprised of a 1k × 1k array of 16 µm 6-Transistor Pinned Photo Diode (6T PPD) pixels. The devices are fabricated on epitaxial silicon and have a depletion depth of 10 µm. The pixel design incorporates a separate photo-node and a very high gain (high sensitivity) ~135 µV/e^- sense node. The high sensitivity pixel enables the device to detect and resolve X-rays with energies well below 1 keV (e.g. for a carbon X-ray which produces on average 77 photo-electrons, the resulting voltage at the pixel would be >10mV). The measured spectral resolution measurements of BM-III

devices are larger than the intrinsic silicon Fano limit at low energies (<1keV) due to incomplete charge collection; nevertheless, the spectral resolution is comparable to other back-thinned X-ray CMOS and CCD imaging spectrometers. The spectral resolution is adequate to fulfill the requirements of SEEJ science. We will characterize the SEEJ CMOS spectral resolution in the energies of interest (~0.3–1.5 keV). The 1k × 1k array consists of two 512 columns × 1k row halves. Each half has its own 512-column-at-a-time, "Clamp-and-Sample" analog Correlated Double Sampling (CDS) processor. Each 512-column processor then reduces to a single buffered output via a 512:1 multiplexer. The maximum possible rate from each output is ~20 Mpixels/sec.

The maximum possible read rate of a full frame, with two output channels operating, is therefore 40 Hz. Smaller regions of interest can be read out at proportionally much higher rates. Further descriptions of the signal chain and pixel design can be found in [37]. The BMIII signal chain provides various readout-modes, including "snap", digital CDS and analog CDS "rolling shutter". For SEEJ operation, it is anticipated to use the analog CDS mode in "rolling shutter" as it is AC coupled and employs the on-chip CDS processor (Fig. 7).

3.2.1 Readout Electronics and data processing

The SEEJ focal plane electronics will consists of four SAO designed CMOS imager headboards, and a centralized CTB. See Fig. 7 for an overall system block diagram. The headboard will be integrated into each MIXO telescope system whereas the separate CTB will be centrally located within the SEEJ spacecraft. The operation of the CMOS detectors will be controlled by an FPGA on the controller/motherboard, via LVCMOS (3.3V levels) buffers and cables. The FPGA provides the necessary pixel row/column addresses and control signals to the CMOS X-ray sensors. One analog video signal from each output buffer of the imager will be routed to a dedicated 10 MS/s ADC on the motherboard. The FPGA clocks the ADCs which in turn provide a stream of serial digital video. The digitized video is read into the FPGA for formatting and further processing (see the firmware description below). The output data will be formatted for further processing to extract only those pixels that contain X-ray photo-charge.

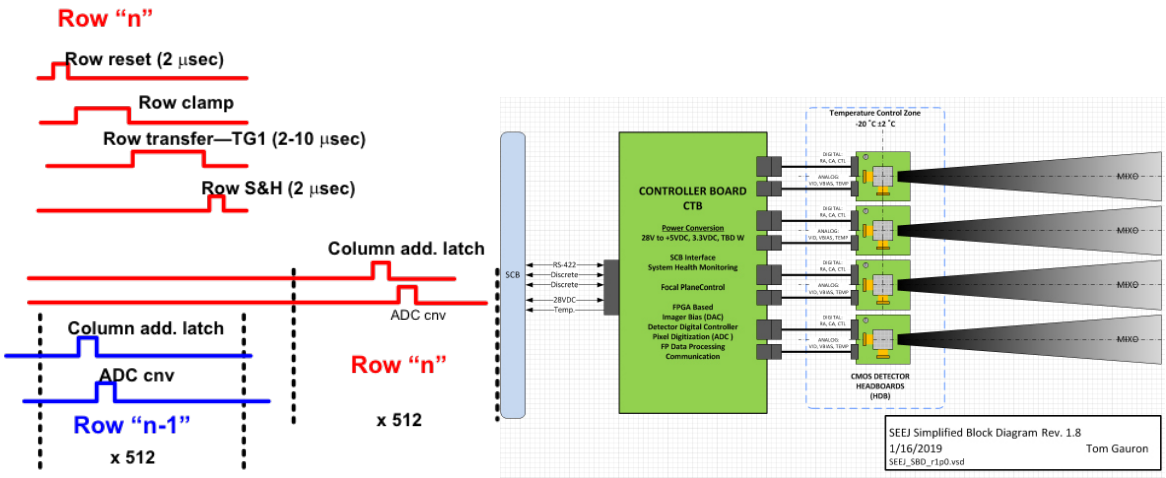

Figure 7: **Left:** Typical readout process using "Clamp-and-Sample" analog Correlated Double Sampling (CDS) processor. The shortest readout time is on the order of 20 µsec. **Right:** Molybdenum flight package (grey) and the two flex circuite (orange), plugging into two flex circuit connectors (brown) on a small interface PWB (green). This board provides a transition to robust wire type connectors (e.g. micro-D) and to the CTB, suitable for the SEEJ mission.

The controller board provides all the primary FPGA voltages required for normal operation of the FPGA and the CMOS imager headboard. Several specific bias voltages will be created and filtered on the headboards using resistor voltage dividers. In particular cases where more current is required (e.g., Pixel Reset), low noise op-amp buffers will be used to increase the drive strength of those bias lines. These voltage dividers, local filtering, and op-amps are located on the headboard so as to be close to the CMOS imager. The controller board will also provide the interface to the spacecraft bus (SCB) for sending science and housekeeping data, control functions, and power conversion from the raw spacecraft power bus.

The software used to process X-ray events detected by the CMOS X-ray sensor, is identical to that of CCD sensors. A median map of several dark frames for the imager array is first generated and stored, then during nominal operation, the

median frame is subtracted from X-ray imaging frames to eliminate any remaining Fixed Pattern Noise (FPN). The FPN corrected X-ray images are then processed to extract X-ray event location and energy.

To compensate for changes in the FPN if any, the FPN map can be (optionally) continuously updated by tracking the median values of the several contemporary several frames. The FPN corrected X-ray images are then processed to extract X-ray event location and energy. The energies of the 3 x 3 pixels around the trigger will be packaged and telemetered along with the pixel coordinates, telescope ID, and time tag. In addition, the CTB will collect various housekeeping (HK) information from the temperature sensors, voltage and current monitors of each CXIS periodically (e.g., every 32 sec), and telemeter them.

4. MISSION & SPACECRAFT

Launching as a secondary payload a rideshare to geostationary orbit (GEO), SEEJ will boot itself to +9000 km above GEO (or higher) to avoid the high electron background present at lower altitudes. Once in orbit SEEJ will observe an average of 1 transit a day for the 12-month study as discussed in S1.

The GEO option is available on a relatively frequent basis and provides a starting point for rapid transit to a scientifically acceptable orbit using a practical OBPS. While GEO is carefully controlled and not allowable for final positioning, any orbit GEO+9000 km is acceptable for science operations and would meet all other ground rules (e.g., acceptable for disposal in place).

The orbit is optimized to allow continuous viewing of targets for several hours at a time to allow uninterrupted viewing of the transit including very good leverage on the baseline pre-and post-transit flux levels. The additional altitude above GEO gets SEEJ above the bulk of the radiation which could otherwise add noise. This orbit maximizes science return while minimizing both cost (multiple available rideshare options, COTS components) and risk (single burn to acceptable operational/graveyard location).

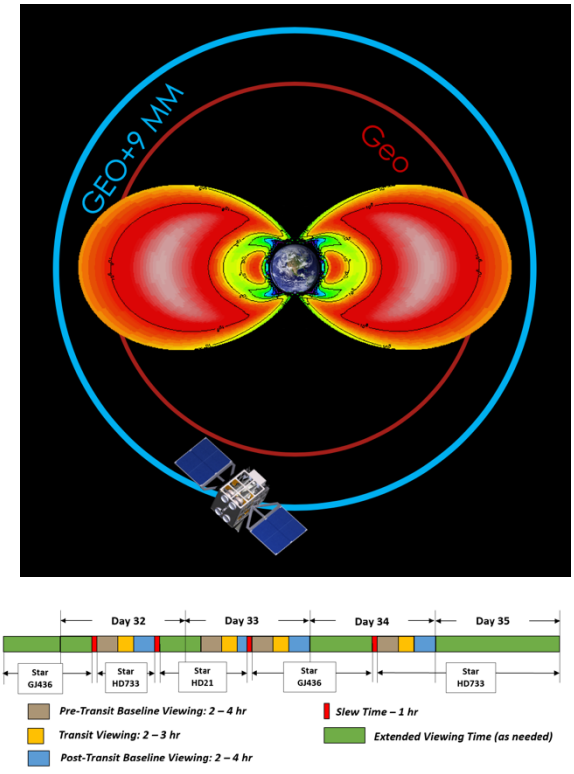

Figure 8: (Top) Baseline orbit for SEEJ. Rideshare to GEO followed by a burn to 9 million meters above GEO. This gets SEEJ safely above the electron belts, shown above in their "maximum" (per AE9;[41]). (Bottom) Baseline observing plan for 4-days of days of the mission.

Science will be performed in transit sequences**.** Each sequence provides 6–11 hours of continuous viewing of a target star. This span is broken down into the following time intervals: A) Typically 4 hours of viewing pre-transit of the hot Jupiter, this establishes the current baseline flux, which is very important since the "quiescent" X-ray flux can vary by a factor of 2 on a moderately active star. B) About 3 hours is assumed for hot Jupiter transfer across front of the star. This is significantly longer than optical transits due to both the inflated size of the planet's atmosphere and the star's corona. C) Up to 4 hours of post-transit viewing, to verify a stable quiescent flux during transit. Following the 11-hour viewing sequence, there are several possibilities: 1) There could be another transit imminent in which case SEEJ would immediately move to that target. In simulations with 8 transits a week visible, we found that, on average, 2 would be overlapping (hence SEEJ could only observe 1) and 3 would be close enough to have some portion of the Pre- or Post- transit observations truncated. 2) SEEJ could stay on the current target to obtain more data at additional synodic and rotational longitudes. 3) Move to a different target to obtain data at synodic longitudes not associated with the transit. 4) Perform calibration observations; effective area, and energy resolution calibrations would be performed at least three times in the primary mission.

5. SPACECRAFT

5.1 SEEJ Spacecraft design details

Based on all mission considerations, a detailed design was developed and a schematic of the planned SEEJ spacecraft showing the major spacecraft systems and the four embedded X-ray telescopes but without solar arrays is shown in Figure 9. The stowed package will fit into one standard ESPA ring slot. Design features of note include the use of four small (1 N), corner-mounted LMP-103S thrusters (to optimize both the thermal environment and spacecraft control) and the symmetrically distributed telescope arrangement (to minimize both spacecraft Guidance, Navigation, & Control (GN&C) requirements and thermal issues).

The power requirements for each spacecraft subsystem (including payload) for the three major flight phases (initial propulsion burn, science operations, and downlink) were calculated. A 30% margin is required in this phase of development and the requirements with margin are shown in the bottom row of the table. The highest value (~ 230 Watts for downlink) set the sizing standard for the SEEJ photovoltaic (PV) array.

Using this requirement, a straightforward PV array was specified. As with all subsystems, the power system design approach mandated exclusive use of COTS components. The power required during eclipse operation is approximately 230 Watts (including margin). The maximum eclipse time for GEO orbit is 73 minutes, or 1.2 hours. Discharge efficiency is 0.95. From this, the energy storage requirement (again with margin) is slightly below 300 Watt-hours (Whr). The allowable battery discharge limit at 65% of capacity based on accepted battery operation practices given the small number of eclipses anticipated over the course of the mission. From this, a total battery capacity of 450 Whr is required. The SAFT microsatellite has a 480 Whr rating, is available as a COTS component and was baselined for the SEEJ spacecraft [38].

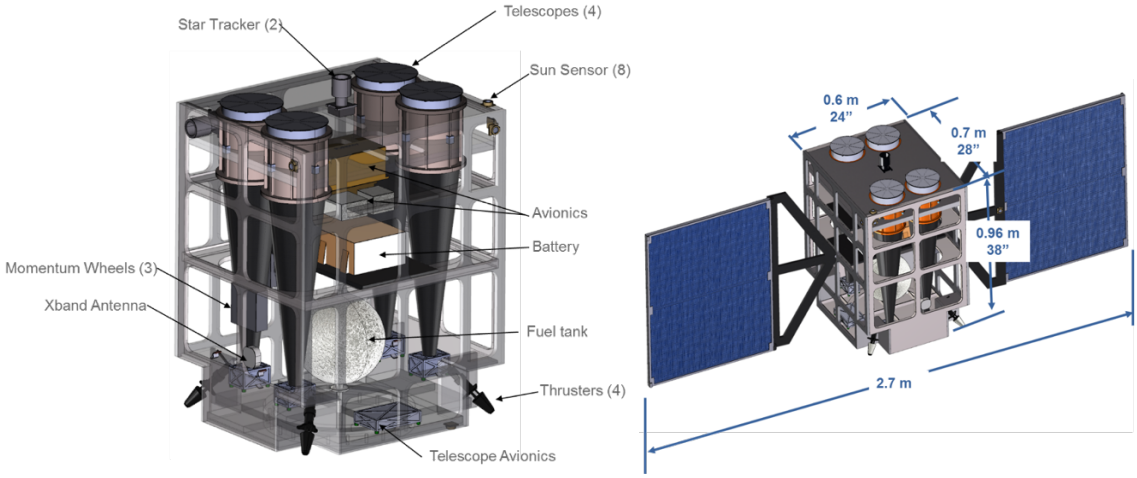

Figure 9: The SEEJ Spacecraft. **Left:** open view. **Right:** SEEJ Spacecraft with solar arrays unfolded.

The Power Management and Distribution (PMAD) requirements are met using three 3U boards that are located with the C&DH subsystem in a common enclosure. For sizing purposes, the study used the Moog Broad Reach suite which is an available COTS article sufficient for the SEEJ application. A single SACI ™ board (shown in Figure 10) performs solar array regulation, battery charge control, battery and array telemetry, and provides an RS422 interface to the Command & Data Handling (C&DH) system. It also provides low voltage (5V) power to the other power boards. PAPI™ and LASI™ boards provide switching to all spacecraft and science loads. All switched circuits have current limit protection and have been flown many times in similar applications.

Structural design of the SEEJ spacecraft BUS assumes simple, mechanically-fastened all aluminum construction. Aluminum honeycomb sandwich panels are used as needed to achieve a stiff yet lightweight design. Each telescope assumes use of a launch lock at the aft end of the spacecraft bus during the launch/ascent phase of the mission. Once on orbit, launch locks are released and the telescopes are mounted to the spacecraft bus only at the forward end. Subsystem components are discreetly represented in the finite element model to properly account for mass and center of gravity.

The avionics and power subsystem analysis efforts were coordinated to assure that electrical power loads of all of the avionic components were included in the power system design. X-band communication was selected for downlink, S-band

for uplink. This selection provides the required communications links at minimum complexity/cost and are compatible with both Near Earth Network (NEN) and Deep Space Network (DSN) assets. For the baseline configuration in the GEO+ orbit, the NEN will be used. The NEN is general used for cis-GEO locations, whereas the DSN is used for greater distances such as cis-lunar and beyond. All NEN station considered have X-band downlink and S-band uplink capabilities. The DSN also has X-band downlink and S-band uplink capability, but with much greater gains using larger dish antennas for the greater distances. Therefore, the same onboard communications system can be used for either location.

For the **Command and Data Handling** (C&DH) and navigation aspects of the avionics design, the strategy was to use of high heritage level components.

Packaging all the avionics control, power, and navigation boards into one enclosure provides the best mass and thermal management efficiencies while also minimizes cabling required. It was found that the COTS Moog/Broad Reach Integrated Avionics Unit (IAU) has similar capabilities as required for this mission. This IAU avionics suite is moderate in cost and has good flight heritage. The IAU is now flying on ANGELS and EAGLE in GEO. In addition to the IAU, a dedicated deployment unit for power management during transit and S/C power up after deployment is included.

To achieve the desired pointing and positional knowledge desired for the mission science, it was decided to add a GPS assisted navigation board to the IAU. The Moog/Broad Reach Nav-SBR board achieves these goals using the GPS enhanced Onboard Navigation System (GEONS), developed by GSFC with the Navigator program. Two Star Trackers are included in the GNC system to provide accurate pointing knowledge in support of the navigation system.

At the selected GEO+ location, the NearEarth Network (NEN) will be used. For analysis, GEO +1,000 km was used, but the results vary only slightly across all cis-GEO locations. At GEO locations, the SEEJ spacecraft will drift slowly over the ground stations, being in contact for about seven days with any one of the selected stations. SEEJ will switch from one NEN ground station to another about every seven days. The four selected ground station are separated approximately equally around the globe, allowing for continuous uninterrupted ground coverage.

Guidance, Navigation, & Control (GN&C): Analysis showed that driving requirement for wheel size was found to be the integrated disturbance torque induced by the solar radiation pressure on the satellite. Note that because radiation pressure is a function of surface area, it is independent of spacecraft mass. A plot showing the anticipated timeline between desaturation maneuvers for a notional GEO-class, *SEEJ*-sized spacecraft is shown in figure 10.

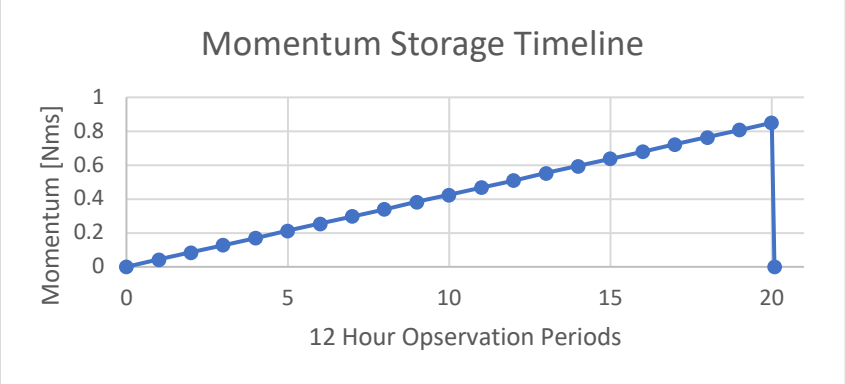

Figure 10: Estimated momentum accumulation and observation periods momentum desaturation maneuvers.

Standard momentum management practice requires momentum dumping via small propulsion system burn once the momentum wheels have reached 85% of their momentum storage capacity. This strategy combined with estimated momentum control requirements (i.e. anticipated saturation rate) and the selected COTS wheels were used to provide propulsion system requirements for the desaturation maneuvers. These calculations show that desaturation burns will be required about 3 times monthly (one approximately every 10.5 days) and that these would require 0.15 kg of propellant. It is noted that momentum dumping at 75% capacity was also considered – it increases safety margin and may be more optimal (due to propulsion system blowdown characteristics) if extended mission operations are considered.

T**hermal** analyses provide confidence that a passive thermal control system based on high-TRL technologies is sufficient to maintain spacecraft avionics and scientific instruments within their operating temperatures. Operating and survival temperatures for spacecraft avionics were assumed based on previous engineering studies, and the desired temperatures for the CMOS and MiXO. The spacecraft requires maintenance of three separate thermal zones for avionics,

the instruments, and the CMOS processors. The strategy for maintaining the CMOS and mirrors at their desired temperature is to cold bias their thermal zones below the specified temperature, so that small, thin-film heaters can be employed to dial-in the appropriate temperatures. Thin film heaters similar to those developed by Minco have been sized to provide sufficient heating to the spacecraft and instruments [39]. The power system budget includes 40W for heating of cold-biased components. The CMOS would be biased to -30°C while the mirror would be biased to 20°C.

The scientific instruments will need to be thermally isolated from the spacecraft body to prevent heat being conducted into the instruments. Torlon® spacers are sized for this purpose. Multilayer insulation blankets are sized for the propellant tank and for additional thermal isolation of the instruments [40].

The Propulsion Subsystem subsystems consists of heritage Moog hardware and ECAPS green propellant thrusters. As a rideshare mission having a non-toxic propellant is a key enabler. A total of four 1N translational thrusters mounted with a slight cant provide the capability for orbit adjust maneuvers and momentum dumping as required after the initial orbit transfer. Moog's line of propellant tanks are a cost-effective and heritage choice for the LMP-103S propellant tank. This tank uses a rolling metal diaphragm to separate the pressurant gas from the liquid propellant to ensure gas-free propellant supplied to the thrusters along with very precise Center of Gravity control. This same tank was launched in December 2018 carrying the same LMP-103S propellant and is currently on orbit. The system is a blowdown system providing a variable feed pressure to the thrusters. Hot fire data and system pressures are used to determine the precise thrust level. The system has a fuel capacity of 8 kg of propellant providing the necessary delta-V to transfer to the GEO + 9000 km orbit.

6. CONCLUSIONS

The recent NASA SmallSat initiative provides an opportunity for a single mission to accomplish ambitious science, while simultaneously fast tracking the development of new technologies at relatively low cost. SEEJ will pack new MiXO optics and X-ray CMOS detectors in a compact spacecraft. Taking advantage of recent developments in X-ray optics and detector technology and a focused science approach, SEEJ can explore regions of exoplanets unavailable to other wavelengths. The SEEJ team is highly experienced, having led key aspects of the instrumentation, operations, and science return from the Chandra, XMM-Newton, OSIRIS-REx and MinXSS missions.

REFERENCES

[1] Poppenhaeger, K., Schmitt, J.H.M.M., Wolk, S.J. 2013, "Transit Observations of the Hot Jupiter HD 189733b at X-Ray Wavelengths." The Astrophysical Journal 773, 62.

[2] Sanz-Forcada, J., Micela, G., Ribas, I., Pollock, A.M.T., Eiroa, C., Velasco, A., Solano, E., Garcia-Alvarez, D. 2011. "Estimation of the XUV radiation onto close planets and their evaporation." Astronomy and Astrophysics 532, A6.

[3] Vidal-Madjar, A., Lecavelier des Etangs, A., Désert, J.-M., Ballester, G.E., Ferlet, R., Hébrard, G., Mayor, M. 2003. "An extended upper atmosphere around the extrasolar planet HD209458b." Nature 422, 143-146.

[4] Ballester, G.E., Sing, D.K., Herbert, F. 2007. "The signature of hot hydrogen in the atmosphere of the extrasolar planet HD 209458b." Nature 445, 511-514.

[5] Penz, T., Micela, G., Lammer, H. 2008. "Influence of the evolving stellar X-ray luminosity distribution on exoplanetary mass loss." Astronomy and Astrophysics 477, 309-314.

[6] Murray-Clay, R.A., Chiang, E.I., Murray, N. 2009. "Atmospheric Escape From Hot Jupiters." The Astrophysical Journal 693, 23-42.

[7] Lecavelier Des Etangs, A., Ehrenreich, D., Vidal-Madjar, A., Ballester, G.E., Désert, J.-M., Ferlet, R., Hébrard, G., Sing, D.K., Tchakoumegni, K.-O., Udry, S. 2010. "Evaporation of the planet HD 189733b observed in H I Lyman-α." Astronomy and Astrophysics 514, A72.

[8] Ben-Jaffel, L., Sona Hosseini, S. 2010. "On the Existence of Energetic Atoms in the Upper Atmosphere of Exoplanet HD209458b." The Astrophysical Journal 709, 1284-1296.

[9] Liang, M.-C., Seager, S., Parkinson, C.D., Lee, A.Y.-T., Yung, Y.L. 2004. "On the Insignificance of Photochemical Hydrocarbon Aerosols in the Atmospheres of Close-in Extrasolar Giant Planets". The Astrophysical Journal 605, L61.

[10] Burrows, A., Ibgui, L., Hubeny, I. 2008. "Optical Albedo Theory of Strongly Irradiated Giant Planets: The Case of HD 209458b." The Astrophysical Journal 682, 1277.

[11] Kulow, Jennifer R.; France, Kevin; Linsky, Jeffery; Loyd, R. O. Parke 2014. "Lyα Transit Spectroscopy and the Neutral Hydrogen Tail of the Hot Neptune GJ 436b." The Astrophysical Journal 786, article id. 132.
[12] Pillitteri, I., Wolk, S.J., Lopez-Santiago, J., et al. 2014, "The Corona of HD 189733 and its X-Ray Activity." The Astrophysical Journal 785, 145.
[13] Fulton, B. J., Petigura, E. A., Blunt, S., & Sinukoff, E., 2018, "RadVel: The Radial Velocity Modeling Toolkit", Publications of the Astronomical Society of the Pacific, 130, 044504.
[14] Fulton, B. J., & Petigura, E. A., 2018, "The California-Kepler Survey. VII. Precise Planet Radii Leveraging Gaia DR2 Reveal the Stellar Mass Dependence of the Planet Radius Gap", The Astronomical Journal, 156, 264.
[15] Lecavelier des Etangs, A., Vidal-Madjar, A., McConnell, J. C., & Hébrard, G., 2004, "Atmospheric escape from hot Jupiters", Astronomy and Astrophysics, 418, L1.
[16] Ehrenreich, David; Bourrier, Vincent; Wheatley, Peter J.; Lecavelier des Etangs, Alain; Hébrard, Guillaume; Udry, Stéphane; Bonfils, Xavier; Delfosse, Xavier; Désert, Jean-Michel; Sing, David K.; Vidal-Madjar, Alfred 2015. "A giant comet-like cloud of hydrogen escaping the warm Neptune-mass exoplanet GJ 436b." Nature 522, 7557, 459.
[17] Dennerl, K., 2006, "X-Rays From Mars", Space Science Reviews, 126, 403.
[18] Voges, W., and 17 colleagues 2000. "Rosat All-Sky Survey Faint Source Catalogue." International Astronomical Union Circular 7432, 3.
[19] Wright, J.T., Marcy, G.W., Howard, A.W., Johnson, J.A., Morton, T.D., Fischer, D.A. 2012. "The Frequency of Hot Jupiters Orbiting nearby Solar-type Stars." The Astrophysical Journal 753, 160.
[20] Wolter, H. (1975). Mirror systems with grazing incidence as image-forming optics for x-rays. *Mirror systems with grazing incidence as image-forming optics for X-rays Transl. into ENGLISH from Ann. Phys. (Leipzig), ser. 6, v. 10, 1952 p 94-114*
[21] Mitsuda, K., Bautz, M., Inoue, H., Kelley, R. L., Koyama, K., Kunieda, H., & Tsunemi, H. (2007). The X-ray observatory Suzaku. Publications of the Astronomical Society of Japan, 59 (sp1), S1-S7.
[22] Takahashi, T., Mitsuda, K., & Kelley, R. (2010, July). The ASTRO-H Mission. In *AIP Conference Proceedings* (Vol. 1248, No. 1, pp. 537-542). AIP
[23] Jansen, F., Lumb, D., Altieri, B., Clavel, J., Ehle, M., Erd, C., ... & Munoz, R. (2001). XMM-Newton observatory-I. The spacecraft and operations. *Astronomy & Astrophysics*, 365 (1), L1-L6.
[24] Pavlinsky, M., Sunyaev, R., Churazov, E., Gilfanov, M., Vikhlinin, A., Hasinger, G., ... & Ohashi, T. (2008, July). Spectrum-roentgen-gamma astrophysical mission. In *Proc. of SPIE Vol* (Vol. 7011, pp. 70110H-1).
[25] Krucker, S., Christe, S., Glesener, L., Ishikawa, S. N., McBride, S., Glaser, D., ... & Saito, S. (2011). The Focusing Optics x-ray Solar Imager: FOXSI. NASA Goddard Space Flight Center; Greenbelt, MD.
[26] Ames, A., Ampleford, D., Bourdon, C., Bruni, R., Kilaru, K., Kozioziemski, B., ... & Walton, C. (2017, August). Characterization of multilayer coated replicated Wolter optics for imaging x-ray emission from pulsed power. In *Optics for EUV, X-Ray, and Gamma-Ray Astronomy VIII* (Vol. 10399, p. 103991X). International Society for Optics and Photonics
[27] Gubarev, M. V., Khaykovich, B., Ramsey, B., Moncton, D., Zavlin, V. E., Kilaru, K., & Crow, L. (2011, August). From x-ray telescopes to neutron focusing. In *Proc. SPIE* (Vol. 8147, p. 81470B).
[28] Gubarev, M., Ramsey, B., O'Dell, S. L., et al. (2012), "The Marshall Space Flight Center development of mirror modules for the ART-XC instrument aboard the Spectrum-Roentgen-Gamma mission", *Space Telescopes and Instrumentation 2012: Ultraviolet to Gamma Ray. Proceedings of the SPIE*, 8443, 84431U
[29] Krucker, S., Christe, S., Glesener, L., et al. (2011), "The Focusing Optics X-ray Solar Imager (FOXSI)", *Proceedings of the SPIE*, 8147, 814705
[30] Romaine, S., Bruni, R., Choi, B., Jensen, C., Kilaru, K., Ramsey, B., & Sampath, S. (2014). "Development of light weight replicated x-ray optics, II." *Space Telescopes and Instrumentation 2014: Ultraviolet to Gamma Ray. International Society for Optics and Photonics*. Vol. 9144, p. 91441H
[31] Hong, J., & Romaine, S. (2016). "Miniature lightweight X-ray optics (MiXO) for surface elemental composition mapping of asteroids and comets". *Earth, Planets and Space*, 68 (1), 35.
[32] Kenter, A., Kraft, R., Gauron, T., & Murray, S. S., 2014. "Monolithic CMOS imaging x-ray spectrometers", High Energy, Optical, and Infrared Detectors for Astronomy VI, 9154, 91540J.
[33] Janesick, J., Pinter, J., Potter, R., Elliott, T., Andrews, J., Tower, J., Cheng, J., & Bishop, J., 2009 "Fundamental performance differences between CMOS and CCD imagers: part III", Astronomical and Space Optical Systems, 7439, 743907.

[34] Janesick, J., Pinter, J., Potter, R., Elliott, T., Andrews, J., Tower, J., Grygon, M., & Keller, D., 2010 "Fundamental performance differences between CMOS and CCD imagers, part IV", High Energy, Optical, and Infrared Detectors for Astronomy IV, 7742, 77420B.
[35] Korendyke, C. M., Vourlidas, A., Plunkett, S. P., et al. (2013), "Development and test of an active pixel sensor detector for heliospheric imager on solar orbiter and solar probe plus", Proceedings of the SPIE, 8862, 88620J
[36] Turtle, E. P., McEwen, A. S., Collins, G. C., Daubar, I. J., Ernst, C. M., Fletcher, L., Hansen, C. J., Hawkins, S. E., Hayes, A. G., Humm, D., Hurford, T. A., Kirk, R. L., Kutsop, N., Barr Mlinar, A. C., Nimmo, F., Patterson, G. W., Phillips, C. B., Pommerol, A., Prockter, L., Quick, L. C., Reynolds, E. L., Slack, K. A., Soderblom, J. M., Sutton, S., Thomas, N., & Bland, M., 2019. "The Europa Imaging System (EIS): High-Resolution, 3-D Insight into Europa's Geology, Ice Shell, and Potential for Current Activity", Lunar and Planetary Science Conference, 3065.
[37] Kenter, A., Kraft, R., & Gauron, T., 2018. "Monolithic CMOS detectors for use as x-ray imaging spectrometers", Society of Photo-Optical Instrumentation Engineers (SPIE) Conference Series, 10762, 1076209.
[38] SAFT, 2007, "Li-ion MicroSat module17 Ah, 480 Wh, 8S3P", www.saftbatteries.com
[39] Minco Technologies, 2019, http://www.alltechelectronics.com/all-tech-products/all-tech-products-line-card/minco-technology/
[40] Donabedian,M., et al., 200, "Insulation" In Gilmore, D.G. (ed). Spacecraft Thermal Control Handbook, 161-205
[41] Ginet, G.P., O'Brien, T.P., Huston, S.L. et al. (2013) "AE9, AP9 and SPM: New Models for Specifying the Trapped Energetic Particle and Space Plasma Environment", Space Sci Rev 179: 579.